ACS Sustainable Chemistry & Engineering

Research Article

pubs.acs.org/journal/ascecg

Simultaneous Dehalogenation and Removal of Persistent Halocarbon Pesticides from Water Using Graphene Nanocomposites: A Case Study of Lindane

Soujit Sen Gupta,[†] Indranath Chakraborty,[†] Shihabudheen Mundampra Maliyekkal,[‡] Tuhina Adit Mark,[†] Dheeraj Kumar Pandey,[†] Sarit Kumar Das,[§] and Thalappil Pradeep*[,†]

[†]DST Unit on Nanoscience and Thematic Unit of Excellence (TUE), Department of Chemistry, Indian Institute of Technology Madras, Chennai 600 036, India

[‡]Environmental Engineering Division, School of Mechanical and Building Sciences, VIT University, Chennai Campus Chennai 600 048, India

[§]Department of Mechanical Engineering, Indian Institute of Technology Madras, Chennai 600 036, India

Supporting Information

ABSTRACT: This paper describes an unusual chemical reaction that takes place on a graphene composite in a concerted fashion. The reaction shows the conversion of a persistent organochlorine pesticide, lindane ($C_6H_6Cl_6$), present in water, to different isomers of trichlorobenzenes (TCBs, $C_6H_3Cl_3$) on the surface of reduced graphene oxide−silver composites (RGO@Ag). The reaction is unique to the composite and does not occur on RGO and nanoparticles of Ag separately. The products of the reaction were isolated and extensively characterized using analytical techniques such as gas chromatography−mass spectrometry, electrospray ionization mass spectrometry, infrared and NMR, which unequivocally confirmed their identity. The as-formed TCBs were removed from the aqueous medium by adsorption on the same composite. Adsorption of lindane is physical in nature, but that of TCBs is through $\pi-\pi$ interactions. The study reveals the unusual chemical reactivity of graphene−metal composites and their potential for water treatment. The uniqueness of the reaction on RGO@Ag is due to the simultaneous removal of three HCl molecules, leading to the formation of aromatic compounds and concomitant formation of silver chloride. Recycling capacity and effect of diverse species present in natural waters were tested for potential applications in sustainable water treatment.

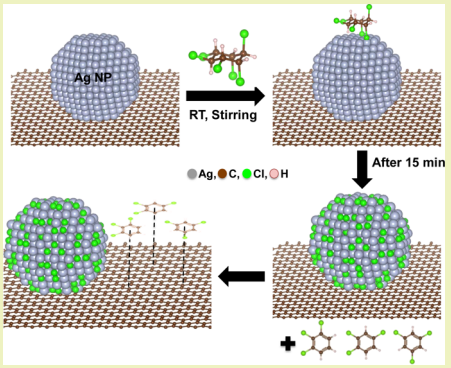

KEYWORDS: *Graphene−silver nanocomposite, Pesticides, Lindane, Degradation, Adsorption, Water purification*

INTRODUCTION

Since its discovery in 2004,[1] graphene has attracted significant attention in various fields due to its unique physical and chemical properties. Though the physicochemical properties[2] and the catalytic behavior[3,4] have been widely investigated, chemistry of its composites has received significant attention these days. Synthesis of different graphene composites, their characterization and applications have been reported in the recent past.[5−7] Molecular adsorption on graphene/graphene based composites and their applications in water purification[8−13] have gained momentum recently. Special properties like large surface area,[14] antibacterial nature,[15−18] reduced cytotoxicity,[19,20] and tunable chemical properties[21] make these materials attractive choices for this application. An overwhelming number of related articles published recently support this claim.[22−33] Attempts are also being made to synthesize graphene from sustainable sources in a cost-effective manner.[9,24,34] This enables the practical use of graphene for a large-scale application like water purification.

To the best of our knowledge, chemical reactions on graphene and graphene nanocomposites enabling the degradation of halogenated pesticides like lindane (γ-hexachlorocyclohexane) are unexplored. Studies report that the degradation of lindane in water using *Streptomyces* sp. M7[35,36] and the fungus *Conidiobolus*[37] is a slow process and takes nearly 5 days of incubation. Degradation using iron(II) sulfide[38] and by iron−palladium bimetallic nanoparticles[39] is also possible, but as cyclohexane is the byproduct, it requires additional methods for further deactivation. Although these are useful, more efforts are needed to develop a better system to enable practical utilitization. The reaction reported here will provide a new methodology for possible decontamination of lindane in water.

In this paper, we report the chemical reactivity of reduced graphene oxide−silver nanocomposites (RGO@Ag) in degrad-

Received: January 30, 2015
Revised: March 30, 2015
Published: May 4, 2015

DOI: 10.1021/acssuschemeng.5b00080
ACS Sustainable Chem. Eng. 2015, 3, 1155−1163

ing halogenated pesticides in water taking lindane (γ-hexachlorocyclohexane) as the model pollutant. There are different isomers of lindane namely α-, β-, δ- and ε-lindane, which are the byproducts during the production of the potent pesticide γ-lindane. γ-Lindane was chosen owing to its widespread occurrence,[40] toxicity[41−43] and persistent nature. According to WHO, the half-life of the γ-isomer ranges from 88 to 1146 days. The paper demonstrates a two-step mechanism of removal, i.e., the degradation of γ-lindane by silver nanoparticles (Ag NPs) supported on RGO and subsequent adsorption of the degraded products by the RGO surface.

MATERIALS AND METHODS

Materials. Natural graphite flakes were procured from Active Carbon India Pvt. Ltd. Sulfuric acid (H_2SO_4, 95−98%), ammonia (NH_3, 30%) and hydrochloric acid (HCl, 36%) were purchased from Rankem Chemicals Pvt. Ltd., India. Hydrazine monohydrate ($N_2H_4 \cdot H_2O$, >99%), phosphorus pentoxide (P_2O_5, 95%), hydrogen peroxide (H_2O_2, 98%) and activated carbon (AC of mesh size 300 nm) were purchased from SD Fine Chemicals Pvt. Ltd., India. Potassium peroxydisulfate ($K_2S_2O_8$, 98%) was purchased from Sisco Research Laboratories Pvt. Ltd., India. Potassium permanganate ($KMnO_4$, 98.5%) was purchased from Merck, India. γ-Lindane (HPLC assay 95%), δ-lindane (purity 99.9%) and multiwalled carbon nanotubes (MWCNTs) were purchased from Sigma-Aldrich. All chemicals were of analytical grade and used as received, without further purification. Two separate 1000 mg/L of lindane (γ-lindane is termed as lindane throughout the text) stock solutions were prepared by dissolving the required quantity of lindane in pure ethanol (99.9%) and *n*-hexane (99.9%) and were kept under refrigerated condition. Working concentrations of lindane were prepared from the stock solutions. A similar procedure was followed to prepare δ-lindane.

Synthesis of RGO@Ag. A procedure similar to the modified Hummers' method[44,45] was used to synthesize graphene oxide (GO) from graphite powder. The reduction of GO to RGO was performed by a chemical route as reported by Li et al.[8,46] Detailed synthetic procedures for GO and RGO are given in the Supporting Information, S1. Working concentrations of RGO were prepared by appropriate dilution of 0.01 wt % stock RGO dispersion. For making RGO@Ag, 100 mL of RGO was taken and calculated amounts of $AgNO_3$ (0.01, 0.05 and 0.1 mM) were added to it to make three different RGO@Ag composites. Each solution was kept undisturbed for 24 h at room temperature (30 ± 2 °C), which allowed the formation of Ag NPs over graphene. The composites were dialyzed using distilled water to remove unwanted ions and then stored in glass bottles for further use. The composites prepared were labeled based on the Ag precursor concentration used [RGO@Ag^{I}, RGO@Ag^{II} and RGO@Ag^{III} for 0.01, 0.05 and 0.1 mM $AgNO_3$, respectively with constant (0.01 wt %) RGO]. RGO@Ag^{I} (hereafter termed as RGO@Ag for simplicity) was used for all experiments unless otherwise mentioned. Inductively coupled plasma mass spectrometry (ICPMS) analysis was done with the filtrate (after the removal of RGO@Ag) to confirm the reduction of Ag^+ to Ag NPs. For RGO@Ag, initially 1.1 mg/L (1.1 ppm) of Ag was used. After the formation of the composite, the amount of silver ions present in the supernatant was found to be less than 1 μg/L (1 ppb). Therefore, it is likely that all Ag^+ was converted to Ag NPs in the presence of RGO, for the formation of the composite. The specific surface area of RGO was measured to be 1215 m^2/g and that of RGO@Ag was 1123 m^2/g.

Adsorption Experiments. All adsorption studies were done in 20 mL batch reactors at room temperature (30 ± 2 °C) keeping 5 mL of RGO@Ag as the working volume. A required amount of lindane stock solution was spiked to the RGO dispersion to get the working concentration of 2 mg/L in all cases unless mentioned elsewhere. The solutions were stirred for a contact time of 15 min. The liquid was separated from the dispersion using a 200 nm membrane filter paper. The filtrate, extracted with hexane, was analyzed for residual lindane and its degradation products using gas chromatography (GC) (PerkinElmer, Clarrus 680) equipped with electron capture detection (ECD). The analysis condition was programmed as follows: run time, 38.5 min; injector temperature, 200 °C; injection rate, 12.5 pts/s and carrier gas flow rate, 1 mL/min. The products were detected using ECD (hexane was used as the solvent for all gas chromatography (GC)-ECD characterizations). The effect of contact time, pH and RGO@Ag dose on the removal of pollutants was evaluated by varying the parameters in the appropriate window. All experiments except kinetics' studies were conducted by batch equilibration method. To test the interference of other ions in the degradation of lindane and removal of the degraded products, studies were also conducted by spiking the required concentration of lindane in tap water (TW). All the experiments were performed in duplicate with proper control and the samples were analyzed immediately.

Instrumentation. UV/vis spectra were measured using a PerkinElmer Lambda 25 UV/vis spectrophotometer. Raman spectra of GO and RGO were collected using a confocal Raman spectrometer (WiTec GmbH CRM 200). RGO and RGO@Ag samples were imaged using a high-resolution transmission electron microscopy (HRTEM) instrument with a UHR polepiece (JEOL 3011, 300 kV) equipped with an analyzer for energy dispersive X-ray analysis (EDAX, Oxford). A scanning electron microscopy (SEM) instrument equipped with EDAX (FEI Quanta 200, Czechoslovakia) was also used to record the surface morphology, elemental composition and elemental maps of the samples. Fourier transform infrared (FTIR) spectra were recorded on a Nicolet 6700 spectrometer. Residual concentrations of lindane in water samples were analyzed using GC-ECD. The mass spectrometric studies were done using an electrospray system, 3200 Q-TRAP LC/MS/MS (Applied Biosystems). GC-ECD and GC−MS measurements give different retention times for the species as the GC parameters are different. Surface area measurements were performed using Micrometritics ASAP 2020 porosimeter, and the Brunauer−Emmett−Teller equation was used to calculate the corresponding values. The concentration of silver ion in the solution was measured using inductively coupled plasma mass spectrometry (ICPMS, NexION 300X, PerkinElmer). X-ray photoelectron spectroscopy (XPS) measurements were done with Omicron ESCA Probe spectrometer with polychromatic Mg Kα X-rays ($h\nu$ = 1253.6 eV). Most of the spectra were deconvoluted to their component peaks using the software CasaXPS. The energy resolution of the spectrometer was set at 0.1 eV at a pass energy of 20 eV. Binding energy was corrected with respect to C 1s at 284.5 eV.

RESULTS AND DISCUSSION

Graphene prepared in the solution phase (RGO) showed a characteristic UV/vis peak centered at 271 nm (blue trace in Figure 1). As RGO characterization has been reported extensively,[8,15,27] we do not discuss this here in detail. RGO@Ag composite was formed through an oxidation−reduction process, in which RGO was oxidized and silver ions were reduced to NPs, which were anchored onto the RGO surface.[8] The recorded UV/vis spectrum of RGO@Ag (red trace in Figure 1) showed the peak corresponding to RGO (269 nm) and an additional plasmonic peak centered around 420 nm, indicating the formation of Ag NPs on the RGO surface. The small blue shift (2 nm) observed for the RGO peak can be ascribed to the partial oxidation of RGO during the reduction of Ag^+ to Ag NPs (an expanded view of UV/vis is shown in the inset of Figure S1 in the Supporting Information). Figure 1 shows the TEM image of RGO@Ag (silver ion concentration 0.01 mM) and the corresponding image for parent RGO is given in Figure S1 of the Supporting Information. The graphene sheets with characteristic nanometer thin wrinkles are clearly visible (marked with white arrows) in the latter image. The sheets are several micrometers in size and the edges and wrinkles are 1.0−1.5 nm thick, corresponding to a bilayer. The black dots seen in the TEM

DOI: 10.1021/acssuschemeng.5b00080
ACS Sustainable Chem. Eng. 2015, 3, 1155−1163

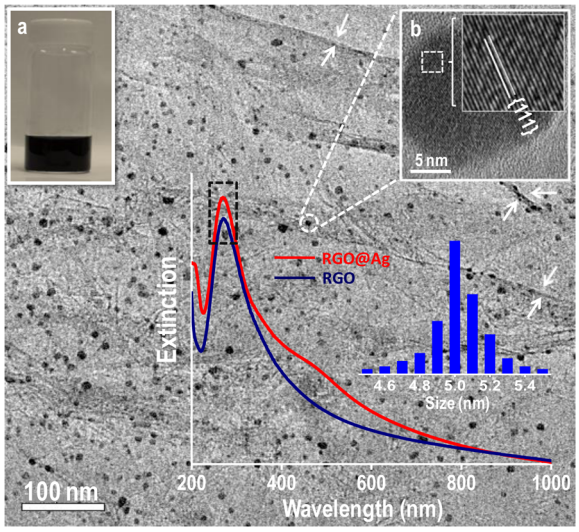

Figure 1. TEM image of RGO@Ag composite (foldings of the RGO sheets are marked with white arrows), the scale bar shows the size distribution of the Ag NPs (5 nm). Inset shows UV/vis spectrum of RGO (blue trace) and RGO@Ag (red trace). Photograph in inset a shows the dispersed nature of RGO@Ag. Inset b is a high resolution image of an Ag particle. Lattice spacing seen in the selected area is expanded further.

image (Figure 1) are due to the presence of Ag NPs over graphene sheets (here also the nanometer thin wrinkles are seen, as the grain boundaries[47]). The well-dispersed particles are almost of uniform size (approximately 5 nm) and spherical in shape. An HRTEM image of one particle is shown in the inset (b) of Figure 1, which shows a lattice spacing of 0.23 nm corresponding to the (111) plane of silver, suggesting that most of the particles are single crystals attached to the RGO sheet. The sizes of the Ag NPs formed are a function of concentration of the silver precursor added initially. An increase in precursor concentration from 0.01 to 0.1 mM of $AgNO_3$ resulted in the formation of particles of size varying from 5 to 50 nm (a detailed discussion is in the Supporting Information, S2, along with TEM images). The graphenic nature of the sheet is intact even after the formation of the composite. The presence of Ag peak in the HRTEM-EDAX spectrum of the composite further confirms the deposition of silver on the RGO sheets (see Figure S2D of the Supporting Information). The XPS spectrum of the RGO@Ag (see Figure S3 of the Supporting Information) composite shows the presence of carbon, oxygen and silver as the only elements. A deconvoluted XPS spectrum of Ag (see Figure S3d of the Supporting Information) shows the $3d_{5/2}$ peak at 368.2 eV, which confirms that silver in the Ag(0) state. Detailed characterizations of these type of RGO composites have been discussed before.[16,34]

To test the reactivity of the composite, RGO@Ag was taken and lindane (dissolved in ethanol from the stock solution) was spiked, such that the final concentration of lindane in the solution was 2 mg/L (ratio of water:ethanol was 500:1 (v/v)). Characterization of the solution was done using GC-ECD and UV/vis at different time intervals to monitor the change in the concentration of lindane in water. Initially, lindane showed a peak around a retention time of 22 min and the solvent peak (hexane) appeared at 3−4 min in the GC-ECD (Figure 2A). With increase in contact time, the lindane peak started to disappear, implying its removal from the solution. Simultaneously, new peaks around a retention time of 5−7 min appeared, which indicated the formation of some products during the process. When the solution was stirred for 15 min, the peaks of both lindane and the products disappeared because of the degradation of the former and the removal of the latter by the RGO@Ag composite, respectively. The UV/vis spectrum in Figure 2B also indicated the formation of some products as the reaction progresses. The kinetic data in the inset of Figure 2B (red trace) predicts that the removal of lindane is a first-order reaction. The removal of lindane was about 99.9% in 15 min. The blue trace in the same inset shows the formation of product in the solution. It is clearly seen that the product so formed first increased with time, reached a maximum and then it was removed by the composite.

Pristine graphene is hydrophobic in nature, but the carboxylic groups[48,49] present in RGO make it hydrophilic, thereby helping in the formation of a stable dispersion in water. The reduction of silver to Ag NPs by RGO does not affect the stability of the dispersion. This is evident from the photograph shown in the inset of Figure 1. When a nonpolar solvent like

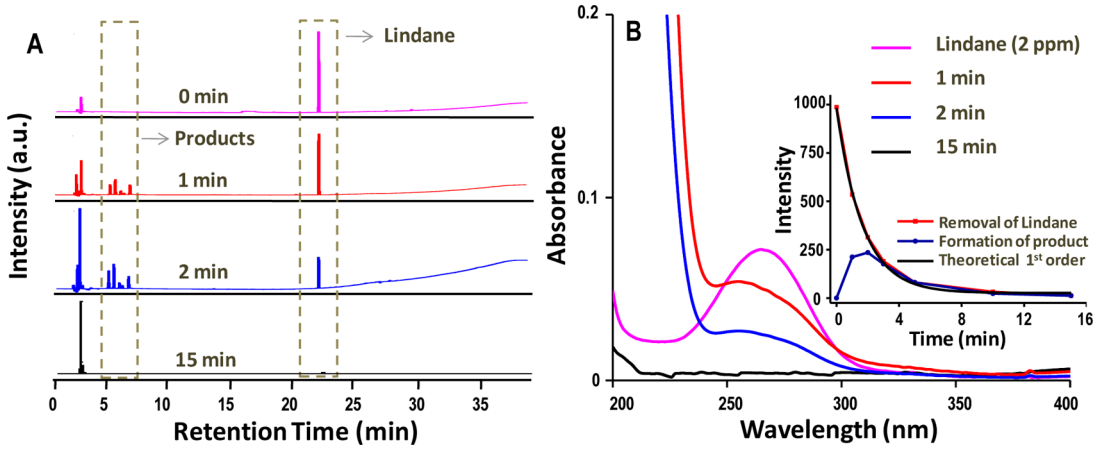

Figure 2. (A) GC-ECD traces and (B) UV/vis data showing the removal of lindane and formation of some products in the solution with respect to time. The dotted areas in A correspond to lindane and product. As can be seen, the lindane peak at the reaction time of 0 min (retention time, 22 min) decreases with time. The peaks of the products increase and then decrease. In panel B, the lindane intensity continuously decreases. The inset in panel B shows the kinetic data for the removal of lindane (red trace) and formation of the product (blue trace).

DOI: 10.1021/acssuschemeng.5b00080
ACS Sustainable Chem. Eng. 2015, 3, 1155−1163

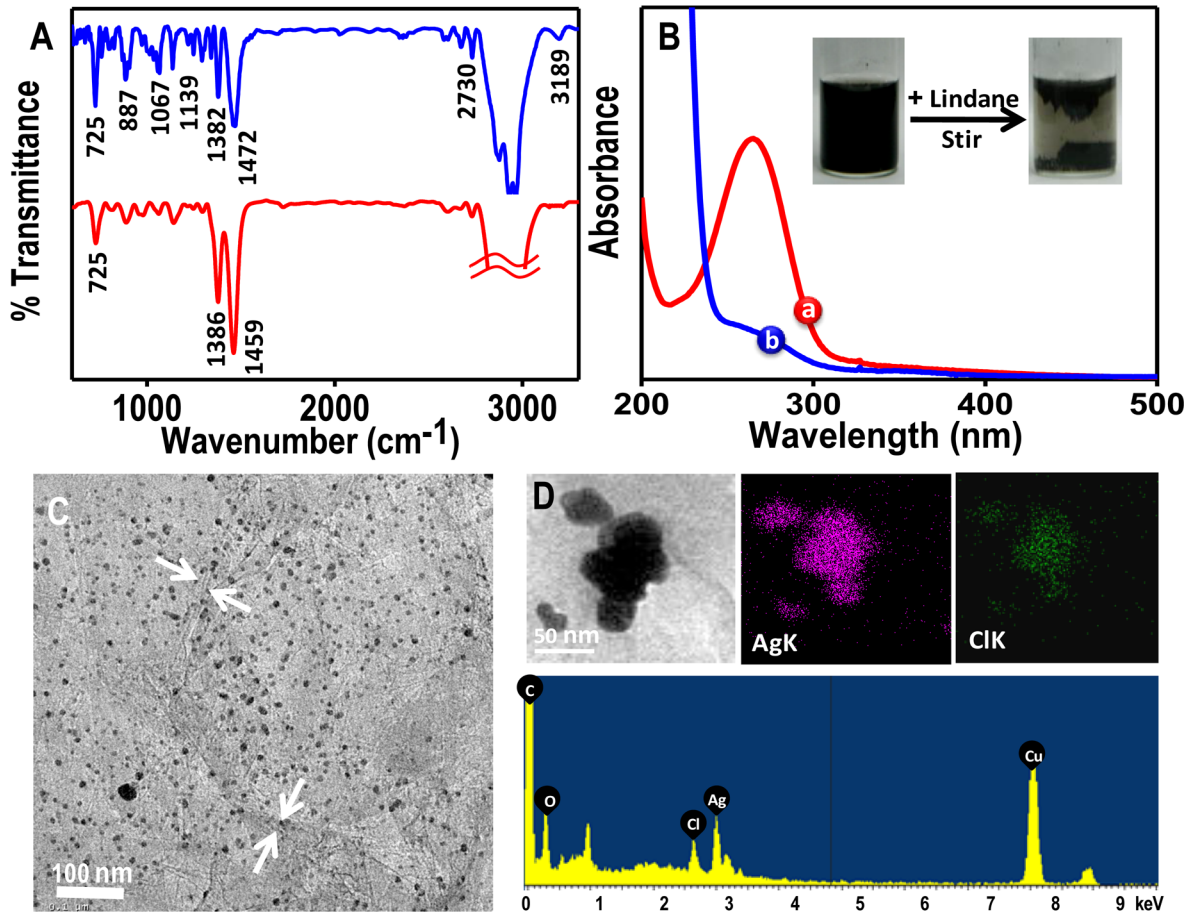

Figure 3. (A) IR spectrum of lindane (red trace) and the product (blue trace), (B) UV/vis spectrum of (a) lindane and the (b) product, inset showing photographs of the reaction mixture before and after reaction, (C) TEM image of RGO@Ag after reaction and (D) TEM-EDAX of the composite after reaction along with elemental mapping data that confirm the presence of silver and chlorine on the surface. Foldings of RGO are marked in panel C.

toluene or hexane is added to RGO dispersed in water, the RGO sheets prefer to stay at the interface and act as interfacial catalysts or reactants; whereas addition of any polar solvent (ethanol/methanol) does not affect their dispersibility. This property helped to isolate the products in the reaction system in the following manner. When lindane (dissolved in hexane) was spiked into the graphene dispersion (0.01 wt %), such that its final concentration was 2 mg/L, the graphene sheets interacted with hexane and lost their dispersibility, as shown in the inset of Figure 3B. Next, the RGO@Ag composites were separated from the solution and extensively characterized with various spectroscopic and microscopic techniques to establish the degradation products; a brief summary of these data is presented below.

The FTIR spectrum of lindane in Figure 3A (red trace) shows a prominent peak at 725 cm^{-1} due to C—Cl stretching and other peaks at 1386 and 1459 cm^{-1} due to rocking and bending vibrations of six C—H groups. The IR spectrum of the product after reacting with RGO@Ag was recorded (Figure 3A (blue trace)). New peaks seen at 887, 1067 and 1139 cm^{-1} are due to the bending vibrations of the =C—H group and the weak peak at 3189 cm^{-1} is due to aromatic C—H stretching. The results give an indication of the formation of an aromatic product. The peak around 2800−3000 cm^{-1} is due to the stretching vibration of O—H present in water. UV/vis data of lindane in hexane shows a prominent peak around 264 nm due to n−σ^* transition, as displayed in Figure 3Ba. The decrease in the intensity of lindane peak after reacting with RGO@Ag (Figure 3Bb) suggests that lindane is getting removed from the solution. It can be further noticed that the absorbance of the solution (Figure 3Bb) starts increasing at 220 nm and continues into the deep UV region (below 200 nm), indicating the formation of a new product in the reaction medium.

A TEM image of was taken after RGO@Ag was reacted with lindane, and an image is shown in Figure 3C. The morphology of the composite does not change even after reacting with lindane. The TEM-EDAX of RGO@Ag after the reaction shows the presence of chlorine (Figure 3D). The elemental mapping of the TEM image in Figure 3D displays that chlorine is present only on silver. The spot SEM-EDAX of the composite confirms the presence of silver along with chlorine (Figure S4 of the Supporting Information) after the reaction. It is also evident from the elemental mapping in the SEM image that there is a one-to-one correspondence with silver and chlorine. In other words, the presence of chlorine is prominent on the surface of silver, which supports the participation of Ag NPs in the degradation of lindane. Similarly, the XPS spectrum of the composite after reaction with lindane shows the presence of AgCl along with C 1s and O 1s (see Figure S5a of the Supporting Information). Figure S5b,c of the Supporting Information shows the deconvoluted spectrum of Cl 2p and Ag 3d, respectively. The deconvoluted XPS spectrum of Ag

DOI: 10.1021/acssuschemeng.5b00080
ACS Sustainable Chem. Eng. 2015, 3, 1155−1163

(see Figure S5c of the Supporting Information) shows the presence of a Ag $3d_{5/2}$ peak at 367.4 eV, which confirms silver in the Ag(I) state.

To confirm the identity of the products, mass spectrometric studies were conducted. As shown in the GC-ECD trace of Figure S6 of the Supporting Information (also in Figure 2), the lindane peak appeared at a retention time of 22 min and the solvent peak appeared around 2−3 min. The occurrence of new peaks (5−6 min) and decrease in the lindane peak as the reaction proceeds indicate the formation of a new molecular species in the reaction medium. Further confirmation comes from the fact that GC−MS analysis of lindane (GC trace in Figure S7A of the Supporting Information, retention time of 12.20 min) shows its molecular ion at m/z 292 (see Figure S8A of the Supporting Information) with isotope distribution for six chlorines, the spectrum matches with that in the literature.[37] The newly formed species, appearing at a retention time of 7.32 min in Figure S8B of the Supporting Information, has a molecular ion peak around m/z 180 (see Figure S7B of the Supporting Information). This can be attributed to the formation of trichlorobenzene (TCB). The isotope pattern with peaks at m/z 179, 181 and 183 is due to the presence of three chlorines in TCB. There is no peak corresponding to m/z 292, indicating the complete degradation of lindane to TCB. It is to be noted that the GC trace showed three distinct peaks for the products (marked as 1, 2 and 3 in Figure S7B of the Supporting Information). The GC−MS of these three peaks is almost similar in nature (given in Figure S9 of the Supporting Information), indicating the existence of TCB isomers in the product.

The product was further confirmed using electrospray ionization mass spectrometry (ESI-MS). Lindane has a set of peaks in the range of m/z 292 (Figure 4A) corresponding to its molecular ion (in the positive mode of ESI). Inset in the figure shows the isotope distribution due to chlorine in the molecular ion (in the positive mode). The degraded product of lindane extracted with hexane was also analyzed by MS (Figure 4B). A set of peaks arising around m/z 180 corresponding to an aromatic benzene ring with three chlorines is observable. The inset in Figure 4B shows the enlarged spectrum in the region of m/z 180 where the isotope distribution for three chlorine atoms can be seen. The calculated spectrum of TCB matches perfectly with the experimental data. To establish the identity of the product, detailed tandem mass spectrometry (MS/MS or MS^2) studies were undertaken. MS^2 analyses of the peaks at m/z 180, 182 and 184 (corresponding to distinct isotopomers of the product) in Figure 4 exhibiting the predicted isotope patterns was conducted at collision energy of 20 (in the instrumental unit). The MS^2 analyses of m/z 179, 181 and 183 are shown in Figure 5a−c. The peaks at m/z 179, 181 and 183

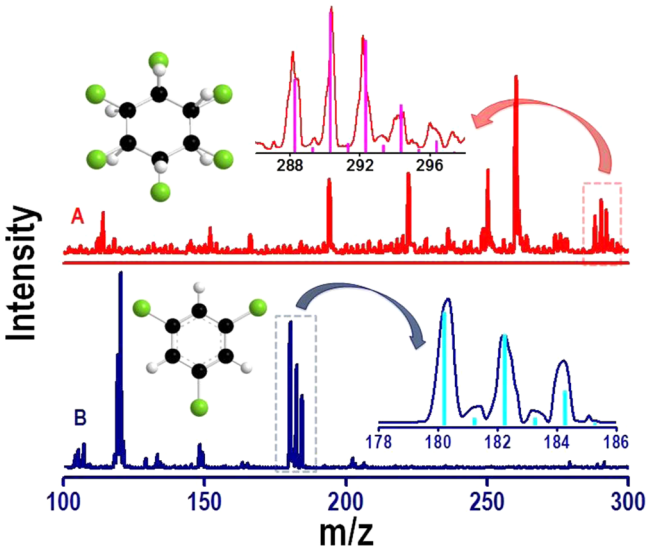

Figure 4. Mass spectrum of (A) lindane (red trace) and the (B) product (blue trace). Inset shows the isotopic distribution of chlorine and the corresponding molecular structure of the analytes.

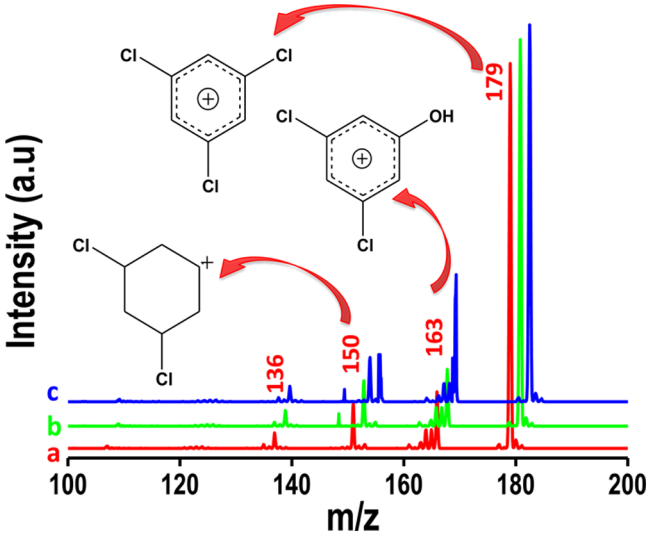

Figure 5. MS-MS of the peaks at m/z 179, 181 and 183 (a, b and c, respectively). The chemical structure of the peak m/z 180, 163 and 150 are shown in the inset. The various isotopologue ions and their fragments are labeled. The ions may have isomeric structures.

in the product are due to $^{35}Cl_3$, $^{35}Cl_2{}^{37}Cl$ and $^{35}Cl^{37}Cl_2$ isotopomers of TCBs (of various isomers), respectively. The MS^2 of the m/z 179 peak (Figure 5 trace a) gives fragments at m/z 163, 151 and 136. The peak at m/z 163 is due to an exchange of one Cl by the OH group from the parent at m/z 179. The peak arising at m/z 151 is due to $C_6H_9Cl_2^+$. Here, ^{35}Cl is lost in fragmentation. In the MS^2 analysis of m/z 181, all the peaks are shifted by two mass units (trace b in Figure 5) higher than in trace a. Two peaks are seen at m/z 153 and 155 in the MS^2 spectrum of m/z 183 (trace c in Figure 5). Here there is a possibility of losing either ^{35}Cl or ^{37}Cl from the parent material. The enlarged full range MS^2 with higher collision energy of 60 is shown in Figure S10 of the Supporting Information.

Next, the reaction with lindane was carried out at a larger scale and the product was collected for further analysis. About 100 mL of RGO@Ag was taken and 1 mL of lindane stock solution (5000 ppm in hexane) was spiked to it. The reaction was carried out for 1 h with continuous stirring. The product was phase transferred to hexane and kept for crystallization for 1 day, after which needle-like crystals were formed (Figure 6Bi, insets). These crystals were characterized extensively. ^1H NMR of lindane (in $CDCl_3$), given in Figure 6A shows the characteristic peak at 4.64 ppm due to the presence of chemically equivalent six C−H bonds. A small peak at 7.26 ppm is due to the solvent, $CDCl_3$. Figure 6B shows the ^1H NMR spectrum of the product, in which the peaks between 7.2

DOI: 10.1021/acssuschemeng.5b00080
ACS Sustainable Chem. Eng. 2015, 3, 1155−1163

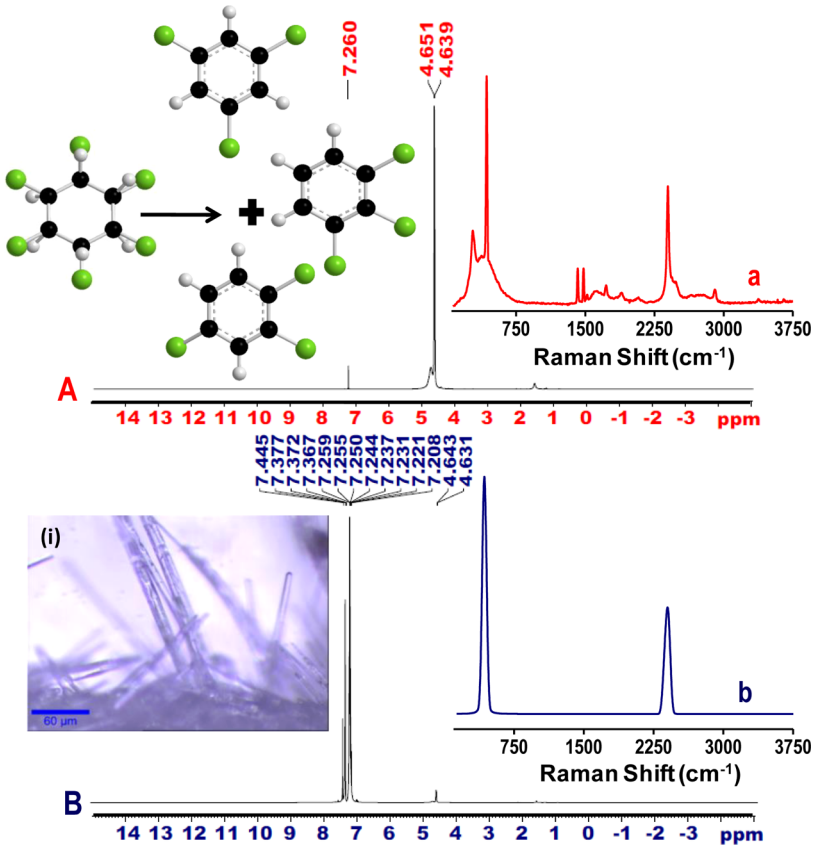

Figure 6. ^{1}H NMR of (A) lindane and (B) the degraded product. The insets show the Raman spectra of (a) lindane and (b) the product. The schematic in panel A shows the structures of lindane and the products. (i) Optical image of the crystals of TCBs is shown.

and 7.5 ppm confirm the presence of aromatic hydrogen. Multiple peaks in the region confirm that a mixture of TCBs is formed in the reaction. The different isomers of TCB are shown in Figure 6A (inset). A weak peak is visible around 4.63 ppm due to the presence of unreacted lindane, which got attached to the crystals when the crystals along with traces of impurities present in the reaction mixture were dissolved in $CDCl_3$. Raman spectrum of lindane in the inset of Figure 6A (Figure 6Aa) shows peaks at 500, 1510 and 1550 cm^{-1}, respectively due to C−Cl and aliphatic C−C stretching modes. In the Raman spectrum of TCBs in the inset of Figure 6B (Figure 6Bb), a peak at 430 cm^{-1} can be seen that confirms the presence of aromatic C−Cl stretching (the image shown here in Figure 6Bb is after baseline correction). The original spectrum has a large fluorescence background due to the conjugated double bond (shown in Figure S11 of the Supporting Information).

Blank tests were performed to check the reactivity of graphene and Ag NPs separately, with lindane. We prepared 50 nm sized citrate capped Ag NPs (Ag@citrate, details of preparation and characterization are given in the Supporting Information, S12). We found that Ag@citrate did not react with lindane, even when kept for 6 h in contact. This can be attributed to the protection of the Ag NPs by the citrate groups, which reduce the accessibility of the silver surface to lindane leading to only a weak interaction between the two. Similarly, RGO did not exhibit any affinity toward lindane. UV/vis spectra in Figure S13A,B of the Supporting Information show that when used independently, Ag@citrate and graphene have a negligible lindane adsorption/degradation capacity. The same reaction was also performed with other carbon materials such as activated carbon (AC), MWCNTs and AC@Ag. A detailed discussion is given in the Supporting Information, S13 on the preparation of AC@Ag. UV/vis data for the removal of lindane by AC@Ag are presented in Figure S13C of the Supporting Information. Corresponding data for the reaction with MWCNTs is plotted in Figure S13D of the Supporting Information. There was little to no degradation or removal of lindane with these materials. Reactivity of lindane toward elemental silver was checked as well. It was found that elemental silver also degraded lindane. However, the capacity of degradation was much higher in the case of the composite (about 100 times) when an equal amount of silver was considered (see Figure S14A of the Supporting Information). Therefore, it is quite clear that the uncapped silver particles are responsible for this unusual dehalogenation. But the conversion efficiency is higher in the case of the composite due to the synergetic effect of Ag NPs on RGO. RGO does not adsorb lindane, but TCBs can adsorb on it, as they have conjugated π-bonds, which are responsible for adsorption.[24,50] The bar diagram in Figure S14B of the Supporting Information compares the different carbon-based materials toward the degradation of lindane and clearly illustrates the uniqueness of RGO@Ag for this dehalogenation reaction.

It is known that silver has a great affinity for halogenated compounds.[51,52] Thus, Ag NPs on RGO react with lindane to form TCBs. This reaction is energetically favorable as the product gains aromaticity, but further degradation of aromatic compounds is thermodynamically unlikely because of the high resonance energy of the benzene ring (152 kJ/mol). Graphene,

DOI: 10.1021/acssuschemeng.5b00080
ACS Sustainable Chem. Eng. 2015, 3, 1155−1163

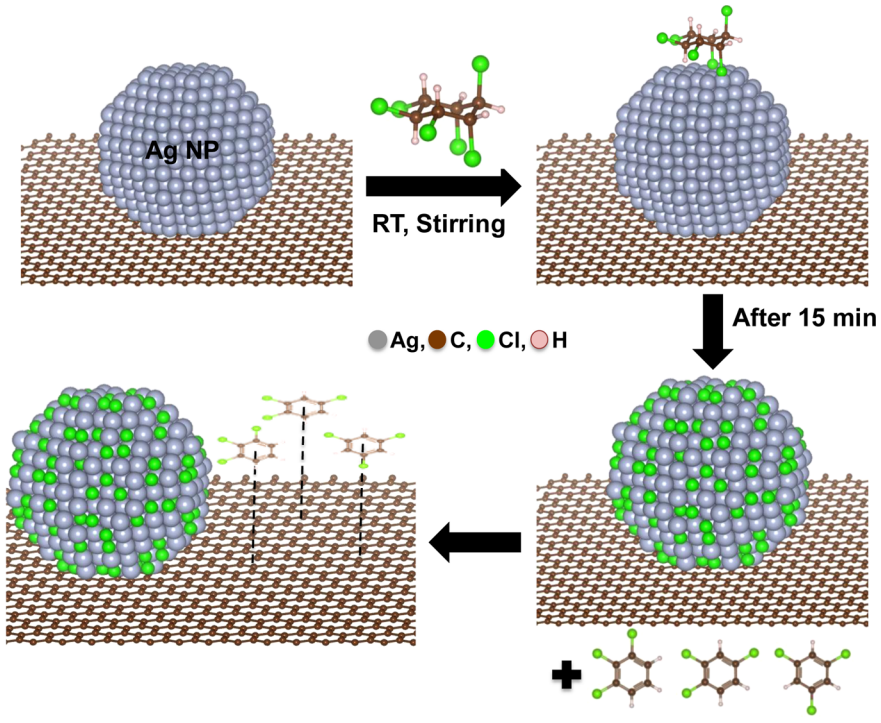

Figure 7. Schematic showing the mechanism of adsorption of lindane on graphene substrate (not to scale).

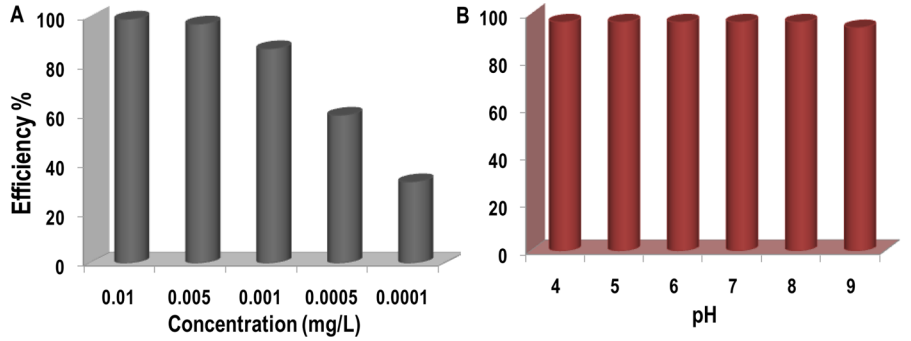

Figure 8. Effect of (A) concentration of the composite and (B) initial pH of the solution on the removal efficiency of lindane.

although promising as an adsorbent, was incapable of removing lindane from the solution when treated alone (see Figure S13B of the Supporting Information). However, it was able to remove TCBs from the solution, as for conjugated organic molecules adsorption occurs via $\pi-\pi$ interactions.[50]

A mechanistic pathway for the degradation of lindane by RGO@Ag is proposed in Figure 7. The figure suggests that when lindane is spiked on RGO@Ag, Ag NPs react with lindane to form different isomers of TCBs. Silver on the graphene substrate changes to AgCl, which remains attached on the graphene sheet. The TCBs formed get adsorbed on graphene sheets by $\pi-\pi$ interactions. Thus, the removal of lindane from water is a two-step process on the RGO@Ag substrate. To confirm that the adsorption of TCBs is physical in nature, they were extracted with a suitable eluent like hexane. About 2 mL of hexane was added to the composite (after the reaction), and the mixture was stirred vigorously for 10 min. The hexane solution was then characterized with GC-ECD, which gave peaks at a retention time of 5−7 min, characteristic of TCBs as shown in Figure 2A. This confirms that the TCBs were weakly adsorbed on the graphene sheets from where they were dissolved in hexane as a result of the vigorous stirring.

Finally, the reaction was evaluated under various conditions to check the viability of the material for practical applications. As mentioned earlier, increase in silver ion concentration during the preparation of RGO@Ag increased the size and concentration of Ag NP on RGO sheets (shown in the TEM image in Figure S2 of the Supporting Information); this is expected to increase the capacity of the composite to degrade lindane (see Figure S15 of the Supporting Information), but we found that capacity with respect to silver loading (in mg/g of silver) toward degradation of lindane is much higher for smaller particles than for bigger particles (see Figure S15 of the Supporting Information). The removal capacity of RGO@Ag was tested upon dilution. It is seen that lower the concentration of the composite, more is the adsorption capacity in mg/g of the material, which is due to the increase in free surface area available upon dilution (Figure 8A). Increased concentrations of the composite may cause the aggregation of graphene sheets. The maximum removal capacity for lindane was found to be 827 mg/g of the composite. Effect of initial pH toward the removal capacity was also examined and it was found that pH did not have any affect in the window of 3−9 (Figure 8B). The pH was maintained acidic or basic using HNO_3 or $NaHCO_3$.

DOI: 10.1021/acssuschemeng.5b00080
ACS Sustainable Chem. Eng. 2015, 3, 1155−1163

The removal capacity decreased with a pH higher than 9 because of the formation of silver hydroxide, which reduces the free silver sites available for the degradation of lindane. The reaction was also performed in TW for real time applications and it showed 70% efficiency compared to the laboratory batch experiments (see Figure S16A of the Supporting Information). The removal capacity of the composite was therefore further examined for common ion effect. For this, 5 mL of RGO@Ag was taken and NaCl solution was spiked to DI water such that the final concentration of the solution was 100 ppm of Cl^-. In the presence of Cl^- ions, the removal efficiency of the composite was found to be 65% versus the laboratory batch experiment, but similar to the efficiency when using TW (see Figure S16B of the Supporting Information). The reaction was also performed with another isomer of lindane (δ-lindane) but no such degradation was observed for this case. Therefore, this type of reaction can open up a new way for isomer selective transformation on graphene substrates, although understanding of the exact mechanism requires additional work. To check the reusability of the composite, repeated adsorption−desorption cycles were performed. For this, the composite was treated with hexane to remove adsorbed TBC and then redispersed in ammoniacal solution through sonication. The analyses of regenerated sample showed no presence of TCB and AgCl. This indicates the possibility of reuse of the material by reloading Ag NPs again on RGO by similar procedure mentioned before. It was seen that the efficiency of the material was around 70−75% even after the fifth cycle of operation (data are presented in Figure S17 of the Supporting Information). Previous studies also show that RGO can be effectively regenerated for repeated use.[17,37]

CONCLUSION

In conclusion, we presented a sustainable and efficient way for dehalogenation reactions on graphene-silver nanocomposites. The conversion of an alycyclic compound, lindane to an aromatic trichlorobenzene was reported for the first time on graphene substrates. In the reaction, lindane was dehydrohalogenated to yield AgCl and different isomers of trichlorobenzene as products that were adsorbed on the graphene substrate by $\pi-\pi$ interactions. This process effectively removed a persistent organochlorine pesticide from water, at efficiency close to 99.9%. It was shown that the high conversion capacity (827 mg/g) observed here for a low concentration of RGO@Ag (0.01 mM) and the recycling ability of the composite could be used effectively for applications in sustainable water treatment. This type of reaction may be employed for the degradation of other toxic halocarbons (studies under progress), which may open up a new method for environmental remediation.

ASSOCIATED CONTENT

Supporting Information

Additional details describing the synthesis of GO and RGO; HRTEM image of RGO and RGO@Ag (at different concentrations of Ag ions); SEM-EDAX image of the composite after the reaction; XPS spectrum of the composite, GC-ECD data showing the removal of lindane; XPS spectrum of the composite after reaction with lindane, GC trace of lindane and the product, GC−MS data of lindane and the degraded product; Raman spectrum of TCBs; synthesis of Ag NPs protected with citrate and their characterization; blank test for RGO, Ag NPs, MWCNTs and AC−Ag composite for the removal of lindane and comparison with elemental silver; dependence of Ag NP size on the degradation of lindane, the effect of tap water and common ion effect on the removal of lindane and the reusability of the material up-to fifth cycle. The Supporting Information is available free of charge on the ACS Publications website at DOI: 10.1021/acssuschemeng.5b00080.

AUTHOR INFORMATION

Corresponding Author

*T. Pradeep. E-mail: pradeep@iitm.ac.in. Fax: 91-44-2257-0545/0509.

Notes

The authors declare no competing financial interest.

ACKNOWLEDGMENTS

We thank the Nano Mission of the Department of Science and Technology (DST), Government of India, for supporting our research program on nanomaterials. SSG thanks the SERB, CII and Thermax India Pvt. Ltd. for a research fellowship. We also thank Jyoti Sarita Mohanty, K. R. Krishnadas, Shridevi Bhat, and Somraj Guha for help in handling different instruments. D.K.P. was a summer fellow from the Department of Chemistry, University of Hyderabad, while part of this work was performed.

REFERENCES

(1) Novoselov, K. S.; Geim, A. K.; Morozov, S. V.; Jiang, D.; Zhang, Y.; Dubonos, S. V.; Grigorieva, I. V.; Firsov, A. A. Electric field effect in atomically thin carbon films. *Science* **2004**, *306*, 666−669.

(2) Geim, A. K.; Novoselov, K. S. The rise of graphene. *Nat. Mater.* **2007**, *6*, 183−191.

(3) Dhakshinamoorthy, A.; Alvaro, M.; Puche, M.; Fornes, V.; Garcia, H. Graphene oxide as catalyst for the acetalization of aldehydes at room temperature. *ChemCatChem* **2012**, *4*, 2026−2030.

(4) Su, C.; Acik, M.; Takai, K.; Lu, J.; Hao, S. J.; Zheng, Y.; Wu, P.; Bao, Q.; Enoki, T.; Chabal, Y. J.; Loh, K. P. Probing the catalytic activity of porous graphene oxide and the origin of this behaviour. *Nat. Commun.* **2012**, *3*.

(5) Gupta, S. S.; Siva, V. M.; Krishnan, S.; Sreeprasad, T. S.; Singh, P. K.; Pradeep, T.; K. Das, S. Thermal conductivity enhancement of nanofluids containing graphene nanosheets. *J. Appl. Phys.* **2011**, *110*, 084302−084306.

(6) Novoselov, K.; Geim, A. K.; Morozov, S.; Jiang, D.; Grigorieva, M. K. I.; Dubonos, S.; Firsov, A. Two-dimensional gas of massless dirac fermions in graphene. *Nature* **2005**, *438*, 197−200.

(7) Georgakilas, V.; Otyepka, M.; Bourlinos, A. B.; Chandra, V.; Kim, N.; Kemp, K. C.; Hobza, P.; Zboril, R.; Kim, K. S. Functionalization of graphene: Covalent and non-covalent approaches, derivatives and applications. *Chem. Rev.* **2012**, *112*, 6156−6214.

(8) Sreeprasad, T. S.; Maliyekkal, S. M.; Lisha, K. P.; Pradeep, T. Reduced graphene oxide−metal/metal oxide composites: Facile synthesis and application in water purification. *J. Hazard. Mater.* **2011**, *186*, 921−931.

(9) Sreeprasad, T. S.; Gupta, S. S.; Maliyekkal, S. M.; Pradeep, T. Immobilized graphene-based composite from asphalt: Facile synthesis and application in water purification. *J. Hazard. Mater.* **2013**, *246−247*, 213−220.

(10) Gao, W.; Majumder, M.; Alemany, L. B.; Narayanan, T. N.; Ibarra, M. A.; Pradhan, B. K.; Ajayan, P. M. Engineered graphite oxide materials for application in water purification. *ACS Appl. Mater. Interfaces* **2011**, *3*, 1821−1826.

(11) Ai, L.; Zhang, C.; Chen, Z. Removal of methylene blue from aqueous solution by a solvothermal-synthesized graphene/magnetite composite. *J. Hazard. Mater.* **2011**, *192*, 1515−1524.

(12) Zhu, J.; Wei, S.; Gu, H.; Rapole, S. B.; Wang, Q.; Luo, Z.; Haldolaarachchige, N.; Young, D. P.; Guo, Z. One-pot synthesis of magnetic graphene nanocomposites decorated with core@double-shell

DOI: 10.1021/acssuschemeng.5b00080
ACS Sustainable Chem. Eng. 2015, 3, 1155−1163

nanoparticles for fast chromium removal. *Environ. Sci. Technol.* **2012**, *46*, 977−985.
(13) Chang, C. F.; Truong, Q. D.; Chen, J. R. Graphene sheets synthesized by ionic-liquid-assisted electrolysis for application in water purification. *Appl. Surf. Sci.* **2013**, *264*, 329−334.
(14) Zhu, Y.; Murali, S.; Cai, W.; Li, X.; Suk, J. W.; Potts, J. R.; Ruoff, R. S. Graphene and graphene oxide: Synthesis, properties, and applications. *Adv. Mater.* **2010**, *22*, 3906−3924.
(15) Sreeprasad, T. S.; Maliyekkal, M. S.; Deepti, K.; Chaudhari, K.; Xavier, P. L.; Pradeep, T. Transparent, luminescent, antibacterial and patternable film forming composites of graphene oxide/reduced graphene oxide. *ACS Appl. Mater. Interfaces* **2011**, *3*, 2643−2654.
(16) Liu, S.; Zeng, T. H.; Hofmann, M.; Burcombe, E.; Wei, J.; Jiang, R.; Kong, J.; Chen, Y. Antibacterial activity of graphite, graphite oxide, graphene oxide, and reduced graphene oxide: Membrane and oxidative stress. *ACS Nano* **2011**, *5*, 6971−6980.
(17) Hu, W.; Peng, C.; Luo, W.; Lv, M.; Li, X.; Li, D.; Huang, Q.; Fan, C. Graphene-based antibacterial paper. *ACS Nano* **2010**, *4*, 4317−4323.
(18) Wang, W.; Yu, J. C.; Xia, D.; Wong, P. K.; Li, Y. Graphene and g-C_3N_4 nanosheets cowrapped elemental α-sulfur as a novel metal-free heterojunction photocatalyst for bacterial inactivation under visible-light. *Environ. Sci. Technol.* **2013**, *47*, 8724−8732.
(19) Chang, Y.; Yang, S.-T.; Liu, J. H.; Dong, E.; Wang, Y.; Cao, A.; Liu, Y.; Wang, H. In vitro toxicity evaluation of graphene oxide on A549 cells. *Toxicol. Lett.* **2011**, *200*, 201−210.
(20) Akhavan, O.; Ghaderi, E. Toxicity of graphene and graphene oxide nanowalls against bacteria. *ACS Nano* **2010**, *4*, 5731−5736.
(21) Tuček, J.; Kemp, K. C.; Kim, K. S.; Zbořil, R. Iron-oxide-supported nanocarbon in lithium-ion batteries, medical, catalytic, and environmental applications. *ACS Nano* **2014**, *8*, 7571−7612.
(22) Chandra, V.; Park, J.; Chun, Y.; Lee, J. W.; Hwang, I.-C.; Kim, K. S. Water-dispersible magnetite-reduced graphene oxide composites for arsenic removal. *ACS Nano* **2010**, *4*, 3979−3986.
(23) Gao, H.; Sun, Y.; Zhou, J.; Xu, R.; Duan, H. Mussel-inspired synthesis of polydopamine-functionalized graphene hydrogel as reusable adsorbents for water purification. *ACS Appl. Mater. Interfaces* **2012**, *5*, 425−432.
(24) Gupta, S. S.; Sreeprasad, T. S.; Maliyekkal, S. M.; Das, S. K.; Pradeep, T. Graphene from sugar and its application in water purification. *ACS Appl. Mater. Interfaces* **2012**, *4*, 4156−4163.
(25) Li, H.; Zou, L.; Pan, L.; Sun, Z. Novel graphene-like electrodes for capacitive deionization. *Environ. Sci. Technol.* **2010**, *44*, 8692−8697.
(26) Liu, T.; Li, Y.; Du, Q.; Sun, J.; Jiao, Y.; Yang, G.; Wang, Z.; Xia, Y.; Zhang, W.; Wang, K.; Zhu, H.; Wu, D. Adsorption of methylene blue from aqueous solution by graphene. *Colloids Surf., B* **2012**, *90*, 197−203.
(27) Sreeprasad, T. S.; Pradeep, T. Graphene for environmental and biological applications. *Int. J. Mod. Phys. B* **2012**, *26*.
(28) Hou, C.; Zhang, Q.; Li, Y.; Wang, H. P25-graphene hydrogels: Room-temperature synthesis and application for removal of methylene blue from aqueous solution. *J. Hazard. Mater.* **2012**, *205*−*206*, 229−235.
(29) Cohen-Tanugi, D.; Grossman, J. C. Water desalination across nanoporous graphene. *Nano Lett.* **2012**, *12*, 3602−3608.
(30) Maliyekkal, S. M.; Sreeprasad, T. S.; Krishnan, D.; Kouser, S.; Mishra, A. K.; Waghmare, U. V.; Pradeep, T. Graphene: A reusable substrate for unprecedented adsorption of pesticides. *Small* **2013**, *9*, 273−283.
(31) Fan, L.; Luo, C.; Li, X.; Lu, F.; Qiu, H.; Sun, M. Fabrication of novel magnetic chitosan grafted with graphene oxide to enhance adsorption properties for methyl blue. *J. Hazard. Mater.* **2012**, *215*−*216*, 272−279.
(32) Kemp, K. C.; Seema, H.; Saleh, M.; Le, N. H.; Mahesh, K.; Chandra, V.; Kim, K. S. Environmental applications using graphene composites: water remediation and gas adsorption. *Nanoscale* **2013**, *5*, 3149−3171.
(33) Zhao, G.; Li, J.; Ren, X.; Chen, C.; Wang, X. Few-layered graphene oxide nanosheets as superior sorbents for heavy metal ion pollution management. *Environ. Sci. Technol.* **2011**, *45*, 10454−10462.
(34) Ruiz-Hitzky, E.; Darder, M.; Fernandes, F. M.; Zatile, E.; Palomares, F. J.; Aranda, P. Supported graphene from natural resources: Easy preparation and applications. *Adv. Mater.* **2011**, *23*, 5250−5255.
(35) Benimeli, C. S.; Castro, G. R.; Chaile, A. P.; Amoroso, M. J. Lindane removal induction by *Streptomyces* sp. M7. *J. Basic Microbiol.* **2006**, *46*, 348−357.
(36) Benimeli, C. S.; Fuentes, M. S.; Abate, C. M.; Amoroso, M. J. Bioremediation of lindane-contaminated soil by *Streptomyces* sp. M7 and its effects on *Zea mays* growth. *Int. Biodeterior. Biodegrad.* **2008**, *61*, 233−239.
(37) Nagpal, V.; Srinivasan, M. C.; Paknikar, K. M. Biodegradation of γ-hexachlorocyclohexane (lindane) by a non-white rot fungus conidiobolus 03-1-56 isolated from litter. *Indian J. Microbiol* **2008**, *48*, 134−141.
(38) Paknikar, K. M.; Nagpal, V.; Pethkar, A. V.; Rajwade, J. M. Degradation of lindane from aqueous solutions using iron sulfide nanoparticles stabilized by biopolymers. *Sci. Technol. Adv. Mater.* **2005**, *6*, 370−374.
(39) Nagpal, V.; Bokare, A. D.; Chikate, R. C.; Rode, C. V.; Paknikar, K. M. Reductive dechlorination of γ-hexachlorocyclohexane using Fe−Pd bimetallic nanoparticles. *J. Hazard. Mater.* **2010**, *175*, 680−687.
(40) Senthilnathan, J.; Philip, L. Photocatalytic degradation of lindane under UV and visible light using N-doped TiO_2. *Chem. Eng. J.* **2010**, *161*, 83−92.
(41) Silvestroni, L.; Palleschi, S. Effects of organochloride xenobiotics on human spermatozoa. *Chemosphere* **1999**, *39*, 1249−1252.
(42) Hall, R. C. W.; Hall, R. C. W. Long-term psychological and neurological complications of lindane poisoning. *Psychosomatics* **1999**, *40*, 513−517.
(43) Kouras, A.; Zouboulis, A.; Samara, C.; Kouimtzis, T. Removal of pesticides from aqueous solutions by combined physicochemical processes—The behaviour of lindane. *Environ. Pollut.* **1998**, *103*, 193−202.
(44) Hummers, W. S., Jr.; Offeman, R. E. Preparation of graphitic oxide. *J. Am. Chem. Soc.* **1958**, *80*, 1339.
(45) Kovtyukhova, N. I.; Ollivier, P. J.; Martin, B. R.; Mallouk, T. E.; Chizhik, S. A.; Buzaneva, E. V.; Gorchinskiy, A. D. Layer-by-layer assembly of ultrathin composite films from micron-sized graphite oxide sheets and polycations. *Chem. Mater.* **1999**, *11*, 771−778.
(46) Li, D.; Muller, M. B.; Gilje, S.; Kaner, R. B.; Wallace, G. G. Processable aqueous dispersions of graphene nanosheets. *Nat. Nanotechnol.* **2008**, *3*, 101−105.
(47) Yu, S. U.; Park, B.; Cho, Y.; Hyun, S.; Kim, J. K.; Kim, K. S. Simultaneous visualization of graphene grain boundaries and wrinkles with structural information by gold deposition. *ACS Nano* **2014**, *8*, 8662−8668.
(48) Haubner, K.; Murawski, J.; Olk, P.; Eng, L. M.; Ziegler, C.; Adolphi, B.; Jaehne, E. The route to functional graphene oxide. *ChemPhysChem* **2010**, *11*, 2131−2139.
(49) Si, Y.; Samulski, E. T. Synthesis of water soluble graphene. *Nano Lett.* **2008**, *8*, 1679−1682.
(50) Liu, F.; Chung, S.; Oh, G.; Seo, T. S. Three-dimensional graphene oxide nanostructure for fast and efficient water-soluble dye removal. *ACS Appl. Mater. Interfaces* **2011**, *4*, 922−927.
(51) Bootharaju, M. S.; Pradeep, T. Understanding the degradation pathway of the pesticide, chlorpyrifos by noble metal nanoparticles. *Langmuir* **2012**, *28*, 2671−2679.
(52) Bootharaju, M. S.; Deepesh, G. K.; Udayabhaskararao, T.; Pradeep, T. Atomically precise silver clusters for efficient chlorocarbon degradation. *J. Mater. Chem. A* **2013**, *1*, 611−620.

DOI: 10.1021/acssuschemeng.5b00080
ACS Sustainable Chem. Eng. 2015, 3, 1155−1163